Spectrochimica Acta Part A: Molecular and Biomolecular Spectroscopy 150 (2015) 280–289

Contents lists available at ScienceDirect

Spectrochimica Acta Part A: Molecular and Biomolecular Spectroscopy

journal homepage: www.elsevier.com/locate/saa

Spectral, morphological, linear and nonlinear optical properties of nanostructured benzimidazole metal complex thin films

P.A. Praveen [a], R. Ramesh Babu [a,*], K. Jothivenkatachalam [b], K. Ramamurthi [c]

[a] Crystal Growth and Thin film Laboratory, Department of Physics, Bharathidasan University, Tiruchirappalli 620 024, Tamil Nadu, India
[b] Department of Chemistry, Anna University-BIT Campus, Tiruchirappalli 620 024, Tamil Nadu, India
[c] Crystal Growth and Thin film Laboratory, Department of Physics and Nanotechnology, SRM University, Kattankulathur 603 203, Kancheepuram, Tamil Nadu, India

HIGHLIGHTS

- Computational studies ensure the potentiality of Benzimidazole metal complexes towards third order NLO applications.
- Annealing improves the surface uniformity and reduces the optical scattering losses.
- Thermal induced degradation of both the metal complex thin films have been observed by Raman spectroscopy.

GRAPHICAL ABSTRACT

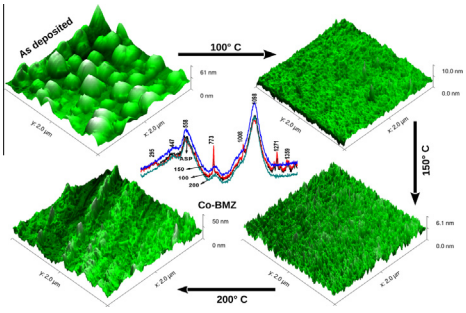

ARTICLE INFO

Article history:
Received 19 February 2015
Received in revised form 19 May 2015
Accepted 24 May 2015
Available online 29 May 2015

Keywords:
Metal organic thin films
Annealing
Nonlinear optical properties
CW Z-scan
Optical limiting

ABSTRACT

Metal organic materials are widely investigated to find their suitability for nonlinear optical applications due to the advantage of combined organic and inorganic properties. In this work benzimidazole based metal organic thin films of dichlorobis (1H-Benzimidazole) Co(II) and dichlorobis (1H-Benzimidazole) Cu(II) were deposited by chemical bath deposition method. The deposited films were annealed at 100, 150 and 200 °C to investigate the effect of annealing on the properties of thin films. Surface homogeneity of the films was increased with the annealing temperature due to the surface diffusion of the films and the same was evidently shown by Raman spectroscopy and Atomic Force Microscopy studies. But annealing the films at 200 °C yielded bulk patches on the surface due to the distortion of molecules. Linear and nonlinear optical properties of the films annealed at 150 °C showed relatively higher transmittance and improved nonlinear optical properties than the other as prepared and annealed samples.

Introduction

Nonlinear optical (NLO) materials with larger hyperpolarizabilities have been investigated for applications in optical switching, signal processing and optical limiting [1,2]. Organic π conjugated materials have been widely investigated due to their better nonlinear optical susceptibilities than the inorganic NLO materials. Organic materials offer low cost fabrication and flexible design possibilities [3,4]. But, the main disadvantages of organic materials are lack of good thermal and mechanical durabilities, and exhibit more optical scattering losses. To overcome these difficulties metal organic materials are considered as the better alternatives due to their versatile molecular configuration, which often enhances the physical properties and provides high laser damage threshold than their organic counterparts [3]. The NLO properties of these materials can be tuned by altering the metal-ligand combinations [5,6]. Depending on the electronegativity, metal centers in the

* Corresponding author. Tel.: +91 431 2407057; fax: +91 431 2407045.
E-mail address: rampap2k@yahoo.co.in (R. Ramesh Babu).

http://dx.doi.org/10.1016/j.saa.2015.05.074
1386-1425/

metal-organic systems can create additional energy levels and electronic transitions other than the $\pi-\pi$ transitions [7]. Especially, the metal ions introduced in a π-conjugated system largely contribute to the charge transfer mechanism between metal and ligand, which can enhance the third order nonlinear optical susceptibility of the materials [8]. NLO materials can be prepared in various forms such as crystals, nanoparticles, polymer composites, thin films, etc. Most often, thin films are considered as suitable candidates for device applications due to their portability, compatibility with silicon photonics and planar waveguides, and their low optical path lengths, which considerably reduces the scattering losses. [9]

Benzimidazole (BMZ), an organic small molecular compound falls under the heterocyclic aromatic category, is well known for its anti-microbial activities [10]. In the recent past, BMZ and its derivatives gain much interest in materials science regime and investigated for the optical, gas, dye sensing and cancer treatment related applications [11–13]. Especially, it is identified as one of the potential second harmonic generation (SHG) materials since it possesses 4 times the SHG efficiency of the standard potassium dihydrogen phosphate (KDP) crystal [14]. Several reports on the coordination behaviour of BMZ with transition metal ions evidently show the ability to tune its properties. Previous works report that incorporation of metal ions in BMZ medium enhances its optical, magnetic and antimicrobial properties [15,10,16]. Further it was reported that the enhancement in the third order nonlinearity can be achieved by the incorporation of Cu or Co metal ions in an organic medium [17]. In this context, we report on the deposition of thin films of dichlorobis (1H-Benzimidazole) cobalt(II) (Co-BMZ) and dichlorobis (1H-Benzimidazole) copper(II) (Cu-BMZ) complexes and characterized them to explore their linear and nonlinear optical properties as a function of annealing temperature.

Materials and methods

All the reagents used in the deposition of Co-BMZ and Cu-BMZ films were purchased from Merck Chemicals. Microscopic glass slides (Labtech) were used as the substrates for film deposition. In the preparation of both the metal complex films, respective metal chlorides ($CoCl_2.6H_2O$ and $CuCl_2.2H_2O$) and ligand (BMZ) were taken in 1:2 ratio. Mixture of methanol and dimethylformamide taken in 3:1 ratio was employed to deposit Cu-BMZ films whereas Co-BMZ films was deposited from ethanol. For depositing films, two glass substrates were fused together by using a sellotape and dipped into the precursor solution, refluxed for 7 h at 70 °C. During the deposition process, the Cu-BMZ solution turns from pale green to dark green and Co-BMZ solution turns to dark blue from pale whitish blue. Then, the deposited films were removed from the solution and dried in a hot air oven at 50 °C for 2 min. The as deposited samples (ASP) were annealed at 100°, 150° and 200 °C (hereafter the samples are termed as 100, 150 and 200) in

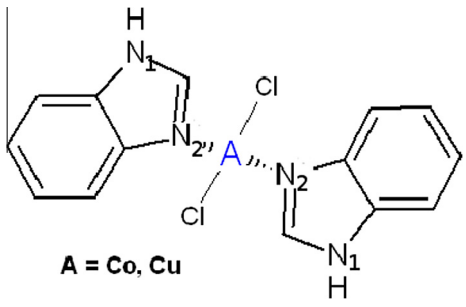

Fig. 1. Chemical Structure of Co-BMZ and Cu-BMZ complexes.

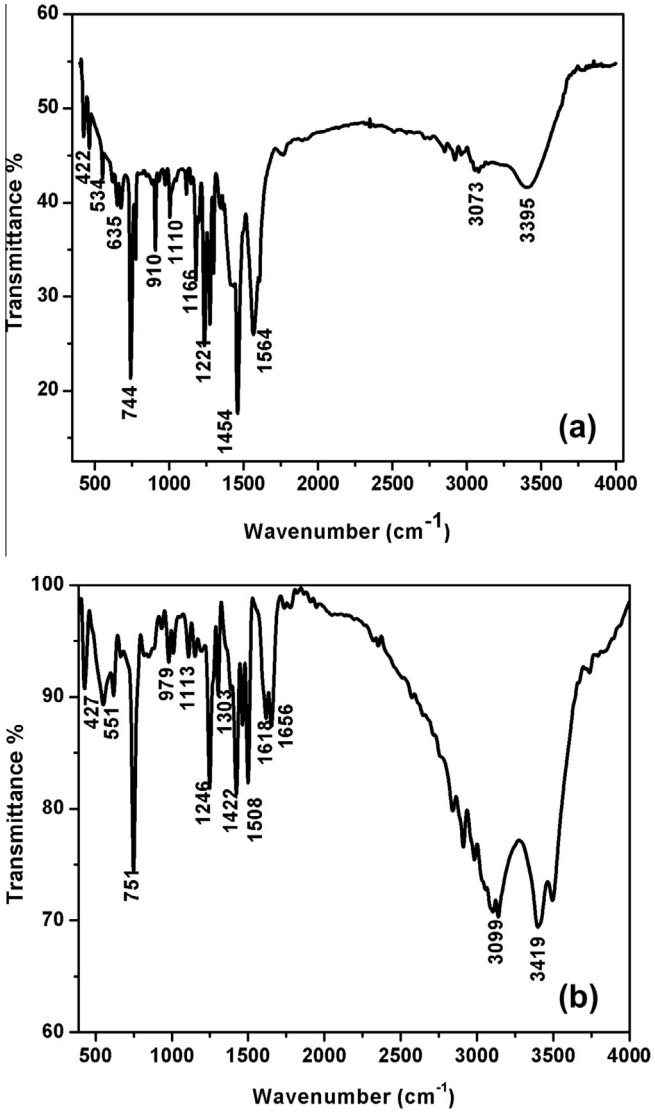

Fig. 2. FTIR spectrum of (a) Co-BMZ and (b) Cu-BMZ.

the open air atmosphere for 2 h, to study the effect of annealing temperature on the surface morphology of the films.

The deposited films were subjected to various characterization studies. Thickness of the samples was determined by simple optical technique [18]. The thickness of Co-BMZ thin films is ~650 nm and that of Cu-BMZ thin films is ~450 nm. Thickness of the thin films decreases with increase in the annealing temperature. The FT-IR spectra were recorded using Perkin Elmer Spectrum RX I system for powders scratched from the deposited films in the range between 400 and 4000 cm^{-1} using KBr pellet technique. Raman spectra of the films were recorded in the range between 200 and 1500 cm^{-1} using Renishaw inVia Reex Raman spectrometer in backscattering geometry. 514.5 nm Ar^+ laser was used as the source and the laser spot size is about 5 μm. The crystallinity of the samples was analysed using XPERT-PRO diffractometer system and the X-ray diffraction pattern of all the samples reveals a broad amorphous hump and no Bragg diffraction peaks were obtained. The pattern is similar to that of a typical amorphous material [19]. Surface morphology of the deposited films were analysed by Atomic Force Microscope (AFM) using SEIKO SPA400-SPI4000 AFM unit in dynamic scanning mode with a scan speed of 0.5 Hz and the radius of the tip is about 10 nm. Transmission spectra of the samples were measured using Perkin Elmer Lambda 35 UV–

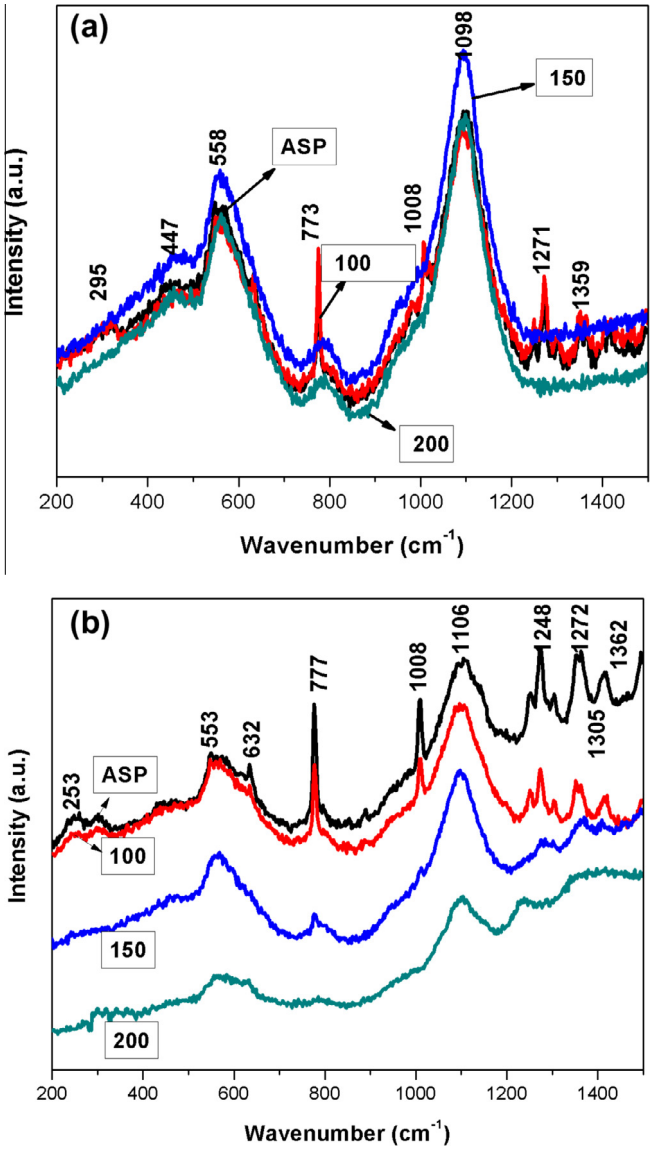

Fig. 3. Raman spectrum of (a) Co-BMZ and (b) Cu-BMZ thin films.

vis spectrometer. The SHG efficiency of the films is recorded by placing the films normal to a Q-switched Nd:YAG laser of wavelength 1064 nm. The relative SHG efficiency of the films deposited in the present work are compared with the results of BMZ thin films of thickness ~500 nm which was reported by Praveen et al. [20]. The third order nonlinear optical properties of the deposited thin films were studied by Z-scan technique at room temperature in open aperture (OA) and closed aperture (CA) configurations [21]. The absorptive and refractive coefficients were used to calculate the magnitude and sign of real and imaginary part of third order nonlinear susceptibility. In the present work, a 20 mW continuous wave (CW) diode laser of wavelength 650 nm was used as the source. A lens of focal length 15 cm was used to focus the beam on the sample and a digital power meter was used to record the variation in output intensity with respect to the sample position (Z). An aperture with linear transmittance of 40% was placed in front of the detector to record the CA scans and it was replaced by a convex lens to record the OA scans. The theoretical relation for transmittance as a function of distance for CA scans can be expressed as [22],

$$T(Z) = 1 - \frac{4.x}{(x^2+9)(x^2+1)}\Phi_0 - \frac{2(x^3+3)}{(x^2+9)(x^2+1)}\Psi_0 \quad (1)$$

where $x = Z/Z_0$, Φ_0 and Ψ_0 is the laser induced phase shift near the focus due to nonlinear refraction and absorption respectively and the Φ_0 is related to the nonlinear refractive index (n_2) by the equation

$$\Phi_0 = kn_2 I_0 L_{eff} \quad (2)$$

where, $k = (2\pi/\lambda)$, I_0 is the intensity of the laser beam at focus ($z = 0$), L_{eff} is the effective thickness of the sample and it can be calculated using the relation $L_{eff} = \frac{(1-e^{-\alpha L})}{\alpha}$, here L is the thickness of the films and α is the linear absorption coefficient of thin films. Eq. (1) is fitted to the experimental data in order to calculate n_2 values. In open aperture Z-scan, the absorption coefficient of the films can be related to transmittance using the relation [22],

$$T(Z) = \sum_{m=0}^{\infty} \frac{[-q_0(Z)]^m}{(m+1)^{3/2}} \quad (3)$$

where $q_0 = \beta I_0 L_{eff}/(1 + (Z^2/Z_0^2))$, β is the nonlinear absorption (NLA) coefficient, Z_0 is the Rayleigh radius, which could be obtained from the relation $Z_0 = \pi\omega_0^2/\lambda$, where ω_0 is the beam waist and λ is the wavelength of source. The value of q_0 is obtained by fitting the Eq. (3) to the experimental data. The real ($Re\chi^{(3)}$) part and imaginary ($Im\chi^{(3)}$) part of the third order nonlinear susceptibility ($\chi^{(3)}$) was calculated using the relation,

$$Re\chi^{(3)} = 2n^2\epsilon_0 c n_2 \quad (4)$$

and

$$Im\chi^{(3)} = \frac{n^2\epsilon_0 c\lambda\beta}{2\pi} \quad (5)$$

where n is the linear refractive index, c is the speed of light in vacuum and ϵ_0 is the permittivity of free space. Further, the absolute value of $\chi^{(3)}$ was calculated from $\left[(Im\chi^{(3)})^2 + (Re\chi^{(3)})^2\right]^{1/2}$. Materials with good third order nonlinear optical susceptibility can be used as optical limiters. Optical limiters (OL) are the devices, which are transparent for the weak intense light but get opaque for high intense light. Optical limiting can be achieved by nonlinear optical process, either by nonlinear refraction or by nonlinear absorption. The experimental arrangement used to carry out the optical limiting studies is similar to the Z-scan setup except a slight modification, such that a polarizer is placed in front of the sample in order to chop the input intensity on the sample [23].

In addition to the experimental studies, the metal complexes investigated in this work were subjected to computational analysis to develop better understanding on the structure-property relationships. All the quantum chemical calculations were performed using parametrized model number 7 (PM7) algorithm embedded in MOPAC2012 package. Molecular structures of the complexes (Fig. 1) were retrieved from the previous reports [15,24] and drawn using ChemDraw package. The geometry optimizations were performed using gradient norm (GNORM) value of about 0.25 and the optimized geometries were subjected to vibrational analysis to ensure that the stable state was achieved. Polarizability (α), first and second hyperpolarizability (β_{SHG}, γ) calculations were carried out at time-dependent Hartree Fock (TDHF) level. Since the knowledge of frontier orbitals are essential to develop complete understanding of hyperpolarizabilities which arise in the molecular structures, the highest occupied molecular orbital (HOMO), lowest unoccupied molecular orbital (LUMO) and the bandgap energies of the Co-BMZ and Cu-BMZ molecules were calculated from the MOPAC .aux file, generated during geometry optimization, using Gabedit molecular plotting program.

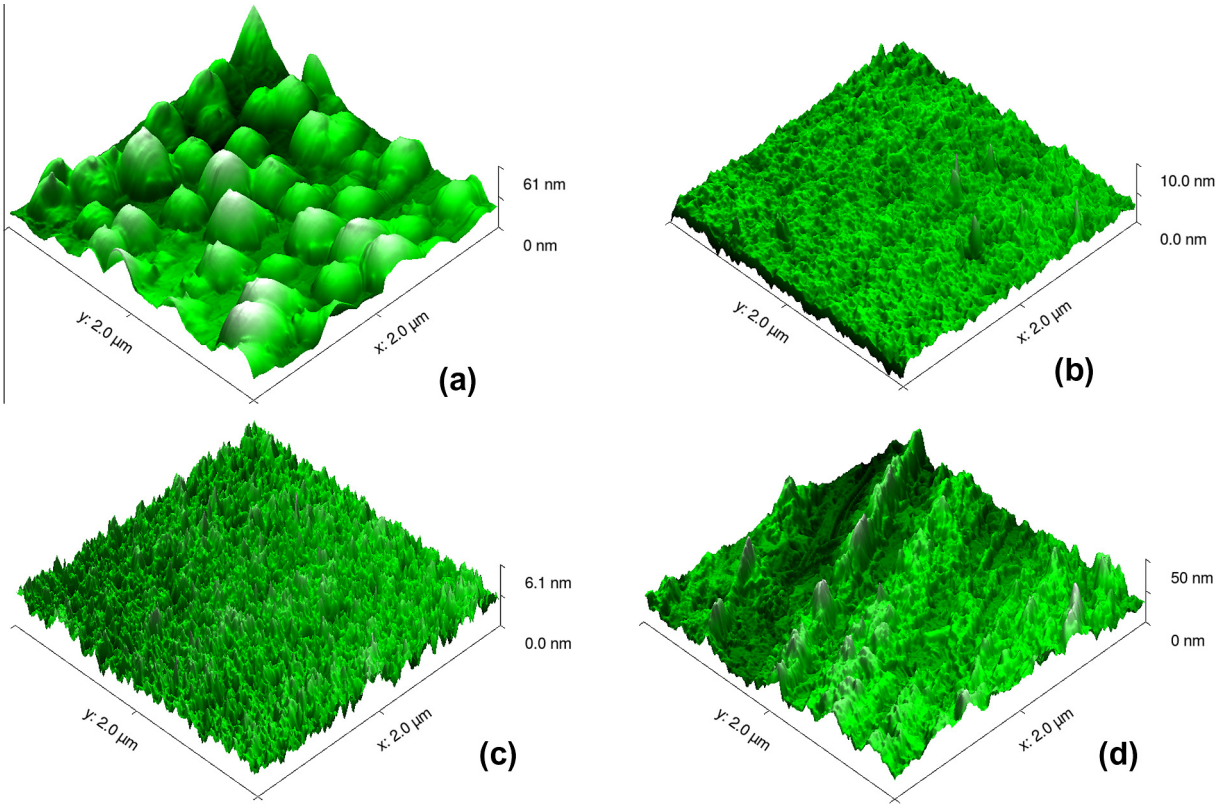

Fig. 4. Surface topography of Co-BMZ thin films: (a) as prepared, annealed at (b) 100 °C (c) 150 °C and (d) 200 °C.

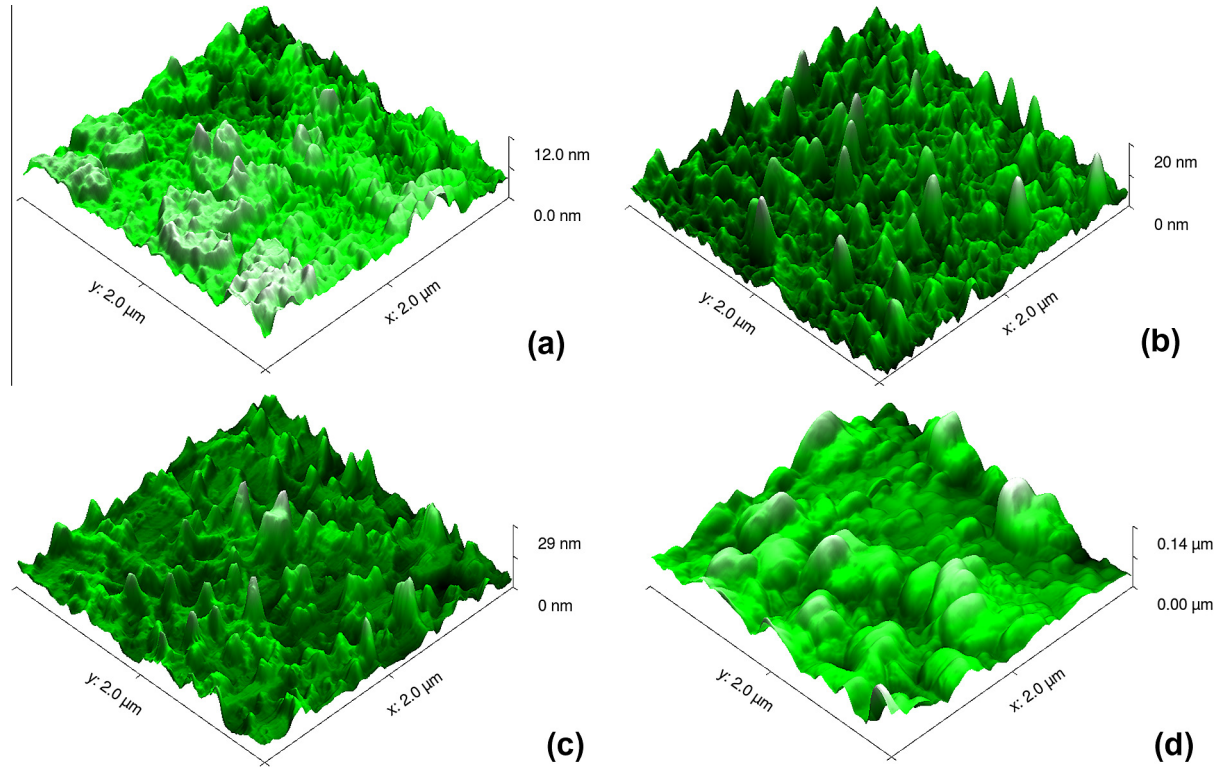

Fig. 5. Surface topography of Cu-BMZ thin films: (a) as prepared, annealed at (b) 100 °C (c) 150 °C and (d) 200 °C.

Table 1
Grain size, RMS, Skewness and Kurtosis values of the Co-BMZ and Cu-BMZ films.

Sample	Grain size (nm^2)		RMS value (nm)		Skewness		Kurtosis	
	Co-BMZ	Cu-BMZ	Co-BMZ	Cu-BMZ	Co-BMZ	Cu-BMZ	Co-BMZ	Cu-BMZ
ASP	21.41	4.04	11.86	2.18	0.60	0.01	−0.23	−0.49
100	3.54	5.74	0.57	2.65	0.40	1.35	4.04	2.79
150	2.64	7.50	0.63	3.63	0.01	1.45	0.15	3.25
200	13.82	44.10	7.48	22.10	0.46	0.71	0.17	0.16

Results and discussion

Structural analysis

In the present work, functional groups of the deposited films were investigated using Fourier Transform Infrared (FTIR) and Raman spectral studies and compared with the previous reports [15,24–27]. Generally, metalated bis-BMZ (M-BMZ) molecules show a slight shift in the FTIR spectrum compared to that of benzimidazole's spectrum. This shift corresponds to the electronegativity of the incorporated metal. In the present case, the shift in the M-BMZ peak positions in FTIR spectra (Fig. 2(a) and (b)) indicates the formation Co-BMZ and Cu-BMZ metal complexes. The peak at 422 cm^{-1} and 427 cm^{-1} in Co-BMZ and Cu-BMZ spectrum, respectively confirms the presence of metal-ligand vibrations. Major changes observed in the ring modes of Co-BMZ and Cu-BMZ molecules compared to that of BMZ can be attributed to the metal-nitrogen interactions. Presence of N–H vibrations at 1110 and 615 cm^{-1} in Co-BMZ, and 1113 and 650 cm^{-1} in Cu-BMZ indicates that the N–H bond at N1 position remains unaffected and the metal is coordinated through the molecule by means of N2 atom. Strong absorption peak observed in the region 3600–2400 cm^{-1} of both the spectra is similar to that the BMZ spectrum which is due to the strong intermolecular hydrogen bonding of BMZ in solid state. We limited the FTIR studies only for ASP samples, because of the difficulties in removing the annealed films by scratching. Fig. 3(a) and (b) show the Raman spectra of Co-BMZ and Cu-BMZ films respectively. In Raman analysis, stretching vibrations are observed at 773 and 777 cm^{-1} corresponding to the metal-ligand co-ordination effect. A broad signal appeared in both the spectra in the region between 1000 and 1200 cm^{-1} is due to the stretching vibrations of C=N, in which the N is coordinated to the metal, thus supporting the tetrahedral coordination of metal with BMZ molecules. Further, the recorded spectra confirms the coordination of the metal ions with benzimidazole ligand, through N2 atom (see Fig. 1). All the annealed films were subjected to Raman analysis and they exhibit a significant change from the ASP spectrum. Variation in the intensity of the Raman spectrum of annealed films can be attributed to the thermal degradation of the metal complexes. In the case of Co-BMZ films decrease in peak intensity observed at 773, 1271 and 1359 cm^{-1} can be ascribed to the breaking of hydrogen bonds between the molecules at higher temperature [28]. But in the case of Cu-BMZ films, decrease in peak intensity of the spectra can be attributed to the thermal decomposition of the complex, i.e., bis form is distorted to form a mono BMZ metal complex, similar to the case of quinoline [29].

Surface analysis

Effect of temperature on the surface topography of the films was analysed by AFM studies. Figs. 4 and 5 show the surface morphology of the as deposited and annealed Co-BMZ and Cu-BMZ thin films respectively. The skewness, kurtosis and root mean square roughness (RMS) values were calculated for all the samples and are given in Table 1. These parameters are widely used to identify the changes in surface morphology and used to evaluate the defect sites and growth mechanism of thin film surfaces. Bright grain spots appeared on the images are due to repulsive forces [30] between the tip and surface caused by higher electron density at the particular point of the surface. Fig. 4(a) shows the morphology of the as prepared Co-BMZ sample with an average grain size of 21 nm. Fig. 4(b) and (c) reveal that the surface smoothness increases due to annealing at 100 °C and 150 °C and correspondingly their grain size falls to 3.54 and 2.64 nm, respectively from 21.41 nm of ASP samples. Even though annealing at 150 °C gives better smoothness, the low skewness obtained can be interpreted due to the slight distortion of films at this temperature. At 200 °C the agglomeration of grains leads to the formation of bulk patches. In the case of Cu-BMZ films, the grain size increases with annealing temperature and the surface smoothness of the films decreases. Films annealed at 150 °C shows more peaks on the surface with an average grain size of about 7.5 nm. Cu-BMZ film annealed at 200 °C also shows the massive agglomeration of grains with bulk patches. It is a well known fact that the diffusion coefficient exponentially increases with the temperature. Thus the observed increase in surface homogeneity of the films with increasing temperature can be interpreted to surface diffusion [31]. However, breaking of molecular bonds at higher temperatures leads to the surface distortion of the films [32].

Computational analysis

From the computational analysis, it is found that the metal complexes possess better polarizability and hyperpolarizability values than that of the parent BMZ molecule. Calculated α, β_{SHG} and γ values of BMZ and its metal complexes are tabulated in Table 2. Eventhough both the metal ions (Co and Cu) can improve the NLO properties of an organic medium, copper performs better than that of cobalt and shows higher nonlinear effect. Similar scenario was observed in the previous report [17]. The calculated values of HOMO, LUMO and HOMO-LUMO energy gap (E_g) for Co-BMZ and Cu-BMZ molecules are given in Table 3. From the Fig. 6 the direct participation of metal ion in both the complexes are

Table 2
Calculated Polarizability and Hyperpolarizability values of BMZ, Co-BMZ and Cu-BMZ.

Material	α (a.u.)	β_{SHG} (esu)	γ (esu)
BMZ	94.67	0.23×10^{-30}	0.3603×10^{-35}
Co-BMZ	368.75	0.44×10^{-24}	22.74×10^{-30}
Cu-BMZ	269.02	8.93×10^{-24}	2168.76×10^{-30}

Table 3
Calculated HOMO, LUMO and E_g values in atomic units.

Type	Co-BMZ	Cu-BMZ
HOMO	−0.3182	−0.3599
LUMO	−0.0526	−0.0385
E_g [HOMO-LUMO]	0.2655	0.3214

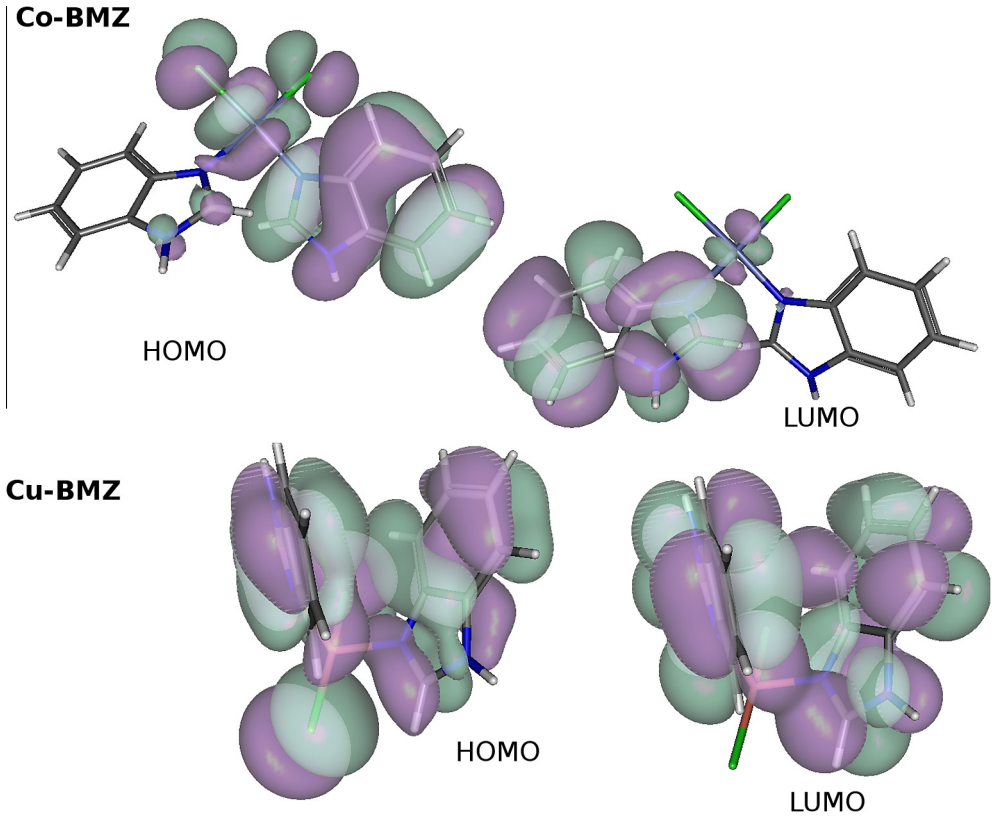

Fig. 6. Frontier orbitals of Co-BMZ and Cu-BMZ molecules.

observed which confirm the contribution of charge transfer excitations, in improving the first and second order hyperpolarizabilities in metalated BMZ when compared with that of BMZ.

Linear optical properties

The linear optical properties of the deposited thin films were analysed by UV–vis. transmission spectrum (Fig. 7(a) and (b)) especially to study their fundamental transitions and optical homogeneity. The as deposited and annealed Co-BMZ films show a broad absorption band in the region of 550–690 nm. This can be assigned to $^4A_2 \rightarrow {}^4T_1$ (P) electronic transition [33]. The band observed in this region is the characteristic of tetrahedral structure and arises due to spin-orbit coupling of the T state. Whereas for Cu-BMZ films, small absorption peaks appeared at about 700 nm can be assigned to the $^2B \rightarrow {}^2E_-$ transition [34]. Both the complexes exhibit strong absorption between 300 and 400 nm corresponding to intra-ligand transitions. The molar extinction coefficient (K) values of Co-BMZ and Cu-BMZ films were calculated using the relation $K = \alpha\lambda/4\pi$, and the calculated K values lie between 220 and 350 for all the samples which support the tetrahedral structure of the complexes [19]. Optical scattering loss often reduces the transmittance and the quality of NLO studies. In the present case, the high transparency of both Co-BMZ and Cu-BMZ thin film complexes ensures its optical homogeneity over a broad spectrum and expected to yield better NLO results respectively. The variation in optical transmittance of the samples with respect to annealing temperature can be understood with the help of grain size of the corresponding samples. In the Co-BMZ thin films, the sudden shift in absorption edge may be due to the agglomeration of nano sized grains to form micro patches. For Cu-BMZ samples annealed at 200 °C the grain size rapidly increases which inturn decreases the optical transmittance of the film, similar to the one reported by Hou et al. [35].

Nonlinear optical properties

SHG efficiency

The relative SHG efficiency calculated for the complexes is given in Table 4. Co-BMZ film shows 1.3 times and Cu-BMZ film shows 2.5 times higher SHG efficiency than that of the BMZ films. Annealing upto 150 °C plays a significant role in the improving SHG efficiency of both the metal complex thin films. Further, Cu-BMZ films shows higher relative SHG efficiency than that of Co-BMZ films and the values agree well with the computational results. Optical scattering loss due to surface distortion reduces the SHG efficiency in both the metal complex films annealed at 200 °C.

Third order nonlinearity

Nonlinear absorptive effects. In the third order nonlinear optical studies, the effective length (L_{eff}) of the samples varies between 3.39×10^{-7} and 6.32×10^{-7} m. Laser beam waist has been calculated as 2.5 μm and the corresponding nonlinear absorption coefficient of Co-BMZ and Cu-BMZ films is in the order of $5.1–5.6 \times 10^{-2}$ m/W and $8.5–9.2 \times 10^{-2}$ m/W, respectively. The nonlinear absorptive and refractive coefficient values calculated from the experimental data are given in Table 5. In open aperture scan, the transmittance falls to a minimum at focus ($z = 0$) for both the metalated BMZ complexes (Fig. 8(a) and (b)), thus indicating the nonlinear behaviour is due to reverse saturable absorption (RSA). Even though, the two photon absorption (TPA) can cause similar decrement in transmission at focus, there is only very lesser chance for TPA in a CW regime and the large Z-scan signal indicates the contribution of thermal effects in the samples. In metal-organic

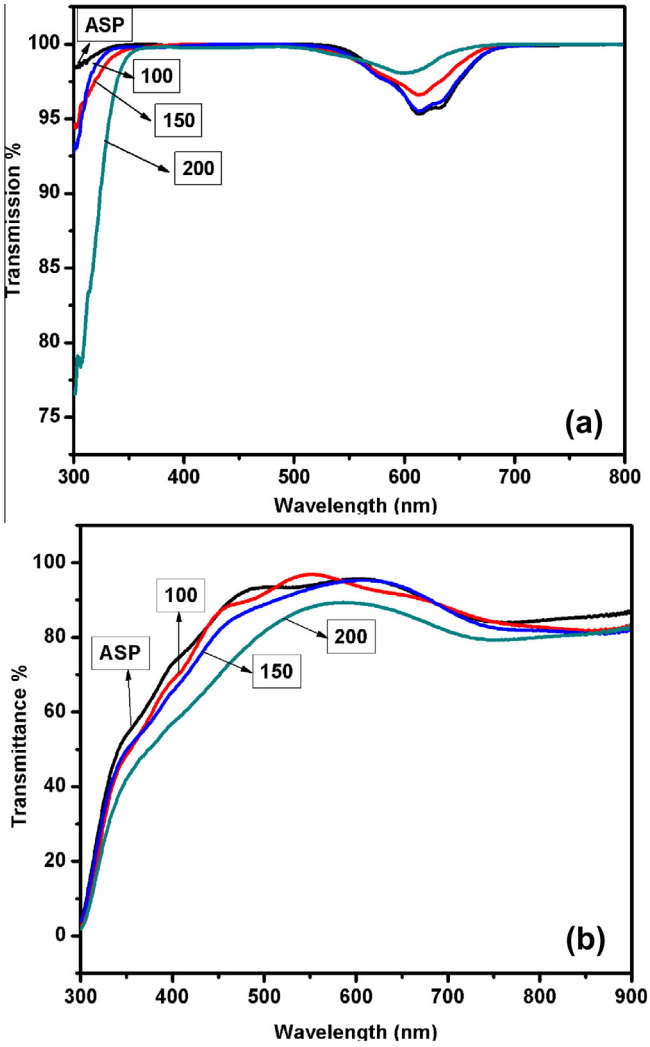

Fig. 7. Transmission spectrum of (a) Co-BMZ and (b) Cu-BMZ samples.

materials the nonlinear optical process can be explained using a five level model diagram [22]. Fig. 9 shows two sets of energy levels S_n and T_n (n = 1,2,3...) of a molecule corresponding to the singlet and triplet states respectively. When the sample was irradiated with a laser source, molecules in the ground state (S_0) get excited to the first electronic excited state (S_1), further they can make a transition to the first triplet state (T_1) by intersystem crossing (ISC) and usually the time scale for ISC is about 1 ns. Upon continuous laser irradiation, molecules in S_1 and T_1 can further get excited to S_2 and T_2 respectively. This type of transitions is referred as the excited state absorption (ESA). In low thresholds the transitions will be on nanosecond scale and the triplet-triplet ($T_1 \rightarrow T_2$) transition plays a dominant role in ESA process and ($S_1 \rightarrow S_2$) transition dominates at higher energies with picosecond time scale limits. Also, if ESA has greater excited state absorption cross section (σ_{ex}) than that of the ground state absorption cross section (σ_0) RSA takes place. On the other hand, if σ_0 is greater than σ_{ex}, saturable absorption (SA) will be observed. Observation of RSA in M-BMZ films suggests that the ESA has greater excited state absorption cross section than that of the ground state absorption cross section and $T_1 \rightarrow T_2$ transition might dominate the RSA process due to the participation of metal ions in the electronic transition. Further, the nonlinear absorption of the samples varies with grain size of the samples. For Co-BMZ samples the nonlinear absorption increases with decreasing grain size whereas for Cu-BMZ films, it increases with increasing grain size. The reason for continuous increment of β in Cu-BMZ films may be due to the optical scattering losses, which reduces the intensity of the output beam. Since there is no way to elucidate the amount of the light scattered by a particular sample, the corresponding change in the intensity is considered as nonlinear absorption effect.

Nonlinear refractive effects. The closed aperture plots of both the complexes imitate the open aperture Z-scan. To extract the nonlinear refractive effects, closed aperture data was divided by open aperture data and the corresponding graphs are shown in Fig. 10(a) and (b) respectively. It can be seen that the Co-BMZ films show a valley–peak (V–P) type curve and Cu-BMZ films show a peak–valley (P–V) type curve. This corresponds to the self defocusing and focusing nature of the thin films, respectively. Results of the present work given in Table 5 reveal that the refractive nonlinear effect is comparatively weaker than the absorptive effects. The nonlinear refractive index of the Cu-BMZ films is found to be negative and hence they can be considered as thin negative lens. On the other hand self focusing effect is observed in Co-BMZ films. In CW regime, thermal effects dominate over other phenomena and variation in nonlinear refractive index of both the complexes can be attributed due to thermal nonlinearity. In the case of Cu-BMZ films, laser heating in absorbing medium, induces a spatial distribution of temperature over the region and this inturn alters the laser beam passing through it. Thus the variation of refractive index is observed due to the strong phase distortion of the propagating beam. While, in Co-BMZ films change in the sign of nonlinear refractive index is due to the variation in excited state population which causes a change in hyperpolarizability of the molecule. High excited state population in the case of Co-BMZ can be attributed to charge-transfer band around 600 nm [36]. Also, the variation in nonlinear refractive index of the samples with respect to annealing temperature can be attributed to the variation in surface homogeneity and grain size of the samples. The nonlinear refractive index of the Co-BMZ films increases with decrease in grain size. Due to the lower grain size values, the optical scattering loss in the medium is reduced and hence the film annealed at 200 °C shows high nonlinear refractive index than that of the ASP sample. In Cu-BMZ film, higher grain size yields high negative nonlinearity. But the variation in n_2 for the samples annealed at 100 and 150 °C may be due to the surface homogeneity and it can be understood from the kurtosis value of the corresponding samples. The third order nonlinear susceptibility of the complex films is in

Table 4
Calculated SHG efficiency of Co-BMZ and Cu-BMZ samples.

Sample	Co-BMZ	Cu-BMZ
ASP	1.31	2.56
100	1.43	2.72
150	1.54	2.91
200	1.32	2.41

Table 5
Calculated nonlinear absorptive and nonlinear refractive coefficients of Co-BMZ and Cu-BMZ thin films from Z-scan.

Sample	β (10^{-2} m/W)		n_2 (10^{-7} m^2/W)	
	Co-BMZ	Cu-BMZ	Co-BMZ	Cu-BMZ
ASP	5.1	8.5	3.76	−3.00
100	5.2	8.8	11.98	−3.74
150	5.4	9.1	12.59	−3.21
200	5.6	9.2	9.81	−14.78

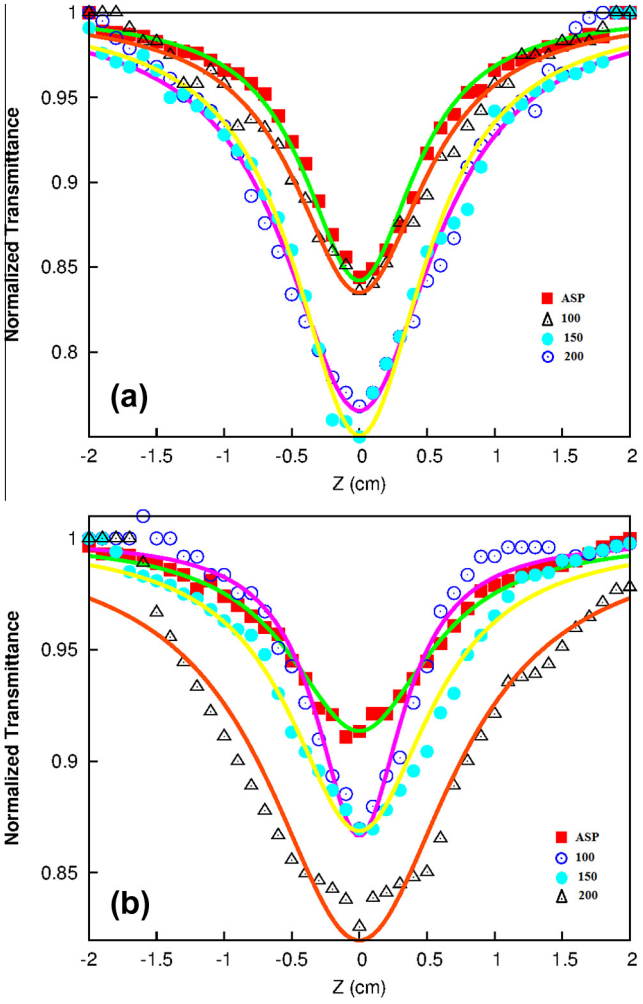

Fig. 8. Open aperture Z-scan curve of (a) Co-BMZ and (b) Cu-BMZ thin films.

the order of 10^{-6} esu. Since the films possess different thickness due to annealing, figure of merit (FOM) for all the samples is calculated by dividing $\chi^{(3)}$ value by their corresponding linear absorption coefficient (α) [21]. From Table 6 it is observed that the Cu-BMZ film possesses high nonlinear optical susceptibility than that of the Co-BMZ films.

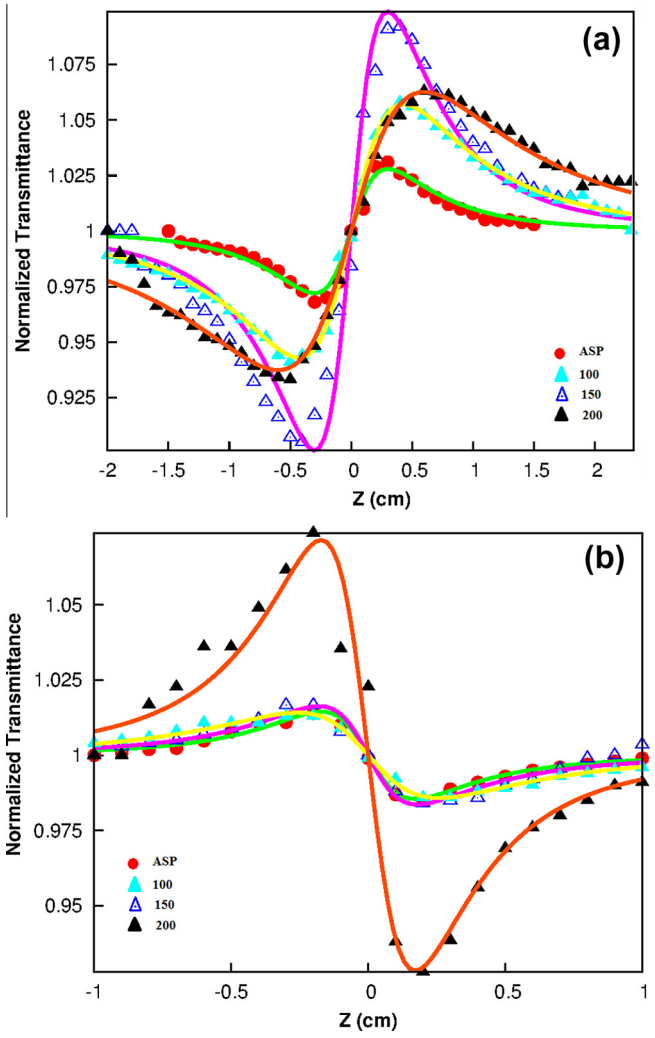

Fig. 10. Closed aperture Z-scan curve of (a) Co-BMZ and (b) Cu-BMZ thin films.

Optical limiting (OL) studies

The Co-BMZ and Cu-BMZ thin films possess strong RSA phenomenon over the nonlinear refraction and they could be investigated for passive OL device applications [37]. The obtained OL

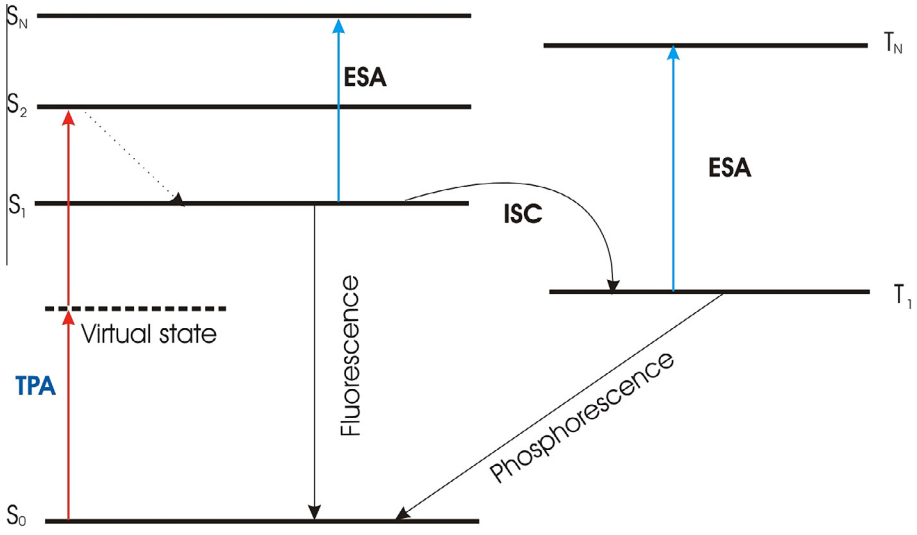

Fig. 9. Five level energy model diagram.

Table 6
Calculated third order nonlinear optical parameters of Co-BMZ and Cu-BMZ thin films from Z-scan.

Sample	Im$\chi^{(3)}$ (10^{-6} esu)		Re$\chi^{(3)}$ (10^{-7} esu)		$\chi^{(3)}$ (10^{-6}) esu		FOM (10^{-13} esu)	
	Co-BMZ	Cu-BMZ	Co-BMZ	Cu-BMZ	Co-BMZ	Cu-BMZ	Co-BMZ	Cu-BMZ
ASP	0.46	9.09	2.23	−5.70	0.68	9.66	0.48	16.15
100	0.49	9.29	6.48	−6.90	1.13	9.98	0.31	21.92
150	0.52	9.32	7.73	−6.07	1.29	9.92	0.94	21.72
200	0.59	9.63	4.19	−7.61	1.00	10.39	0.62	9.94

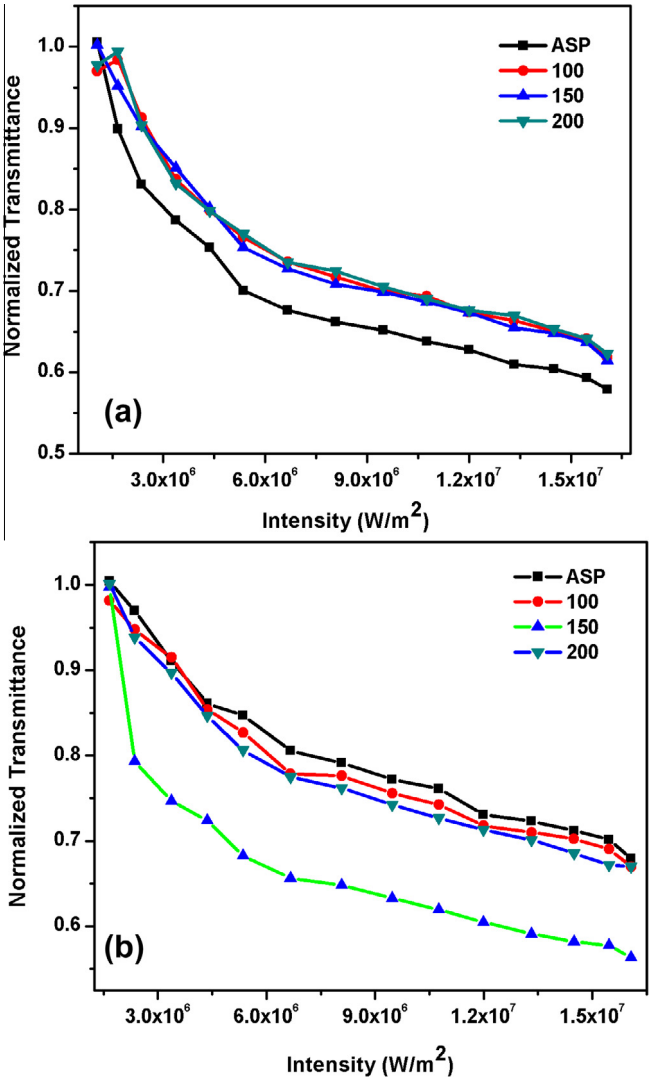

Fig. 11. Optical limiting behaviour of (a) Co-BMZ and (b) Cu-BMZ samples.

results are shown in Fig. 11(a) and (b). At low irradiances the output intensity increases with input intensity but at higher irradiances the medium starts to cease the output and hence the optical limiting is achieved. OL studies show that the films annealed at 200 °C exhibit better limiting behaviour than the other samples due to optical scattering loss.

Conclusion

In the present work, the effect of various annealing temperature on the spectral, linear and nonlinear optical properties of Co-BMZ and Cu-BMZ complex thin films was studied. The presence of metal-nitrogen bond vibartions in FTIR spectra at 422 cm^{-1} in Co-BMZ and 427 cm^{-1} in Cu-BMZ justifies the formation of metal complexes. The metal to ligand charge transfer excitation in the complexes and the highly polarizable nature of the molecules are revealed by the computational studies. The results of Raman spectral studies bring out the annealing induced degradation in these thin film samples. Decrease in the peaks intensity reveals the distortion of H bonds in Co-BMZ and decomposition of Cu-BMZ complex films due to annealing. AFM analysis showed the improved surface homogeneity for the films annealed at 150 °C. Linear optical studies reveal that the films annealed at 100 and 150 °C have better optical transmittance than that of the films annealed at 200 °C. The relative SHG efficiency of the prepared Co-BMZ and Cu-BMZ complex films is higher than that of parent BMZ ligand. The result on Z-scan measurements shows that the nonlinear absorption coefficients of the Co-BMZ films is increased from 0.051 to 0.056 m/W and Cu-BMZ from 0.085 to 0.092 m/W due to the surface defects. Low n_2 values suggest that the domination of nonlinear absorptive effects in the samples at 650 nm of CW laser regime. Third order nonlinear susceptibility of the samples are in the range of 10^{-6} esu and the films annealed at 150 °C acquire better FOM than the other as prepared and annealed samples. In summary, both the metal-organic thin films investigated in this work showed better linear and nonlinear optical properties than their parent ligand and therefore the prepared Co-BMZ and Cu-BMZ complex thin films could be promising candidates for application in nonlinear photonic devices and optical limiters.

Acknowledgements

One of the authors, P.A. Praveen thank the UGC-BSR Govt. of India for financial assistance in the form of Research Fellowship in Science for Meritorious Students (F.4-1/2006/7-197/2007(BSR)).

References

[1] T.J. Kippenberg, R. Holzwarth, S.A. Diddams, Science 332 (2011) 555–559.
[2] J. Olesiak-Banska, M. Gordel, R. Kolkowski, K. Matczyszyn, M. Samoc, J. Phys. Chem. C 116 (2012) 13731–13737.
[3] C.E. Powell, M.G. Humphrey, Coord. Chem. Rev. 248 (2004) 725–756.
[4] S. Barlow, J.-L. Bredas, Y.A. Getmanenko, R.L. Gieseking, J.M. Hales, H. Kim, S.R. Marder, J.W. Perry, C. Risko, Y. Zhang, Mater. Horizons 1 (2014) 1–5.
[5] S.-I. Noro, S. Kitagawa, T. Akutagawa, T. Nakamura, Prog. Polym. Sci. 34 (2009) 240–279.
[6] W.-Y. Wong, Coord. Chem. Rev. 249 (2005) 971–997.
[7] K. Selvaraju, K. Kirubavathi, S. Kumararaman, J. Miner. Mater. Char. Eng. 11 (3) (2012) 303–310.
[8] K. Parasuraman, K. SakthiMurugesan, R. Uthrakumar, S. JeromeDas, B. MiltonBoaz, Phys. B 406 (2011) 3856–3860.
[9] M. Thakur, S. Meyler, Macromolecules 18 (11) (1985) 2341–2344.
[10] E. Sahin, S. Ide, M. Kurt, S. Yurdakul, J. Mol. Struct. 616 (2002) 259–264.
[11] L. Jiang, Z.-X. Li, Y. Wang, G.-D. Feng, W.-X. Zhao, K.-Z. Shao, C.-Y. Sun, L.-J. Li, Z.-M. Su, Inorg. Chem. Commun. 14 (2011) 1077–1081.
[12] S. Samai, K. Biradha, Chem. Mater. 24 (2012) 1165–1173.
[13] A. Paul, R.K. Gupta, M. Dubey, G. Sharma, B. Koch, G. Hundal, M.S. Hundal, D.S. Pandey, RSC Adv. 4 (2014) 41228–41236.
[14] N. Vijayan, G. Bhagavannarayana, G. Budakoti, B. Kumar, V. Upadhyaya, S. Das, Mater. Lett. 62 (2008) 1252–1254.
[15] S. Yurdakul, M. Kurt, J. Mol. Struct. 650 (2003) 181–190.
[16] H. Chang, M. Fu, X.-J. Zhao, E.-C. Yang, J. Coord. Chem. 63 (20) (2010) 3551–3564.
[17] G. de la Torre, P. Vazquez, F. Agullo-Lopez, T. Torres, Chem. Rev. 104 (2004) 3723–3750.

[18] F. Tyler, A Laboratory Manual of Physics, 4th Edition., Edward Arnold Limited, London, 1974.
[19] A.A.M. Farag, I.S. Yahia, Opt. Commun. 283 (2010) 4310–4317.
[20] P.A. Praveen, R. Ramesh Babu, S.P. Prabhakaran, K. Ramamurthi, Bull. Mater. Sci. (accepted manuscript).
[21] V. Krishnakumar, G. Shanmugam, R. Nagalakshmi, J. Phys. D Appl. Phys. 45 (2012) 165102.
[22] S. Zafar, Z.H. Khan, M.S. Khan, Spectrochim. Acta Part A 118 (2014) 852–856.
[23] K. Sendhil, C. Vijayan, M.P. Kothiyal, Opt. Laser Technol. 38 (2006) 512–515.
[24] F.-J. Yoe-Reyes, S. Bernes, N. Barba-Behrens, Acta Crystallogr. Sect. E E61 (2005) m875–m877.
[25] W.-H. Sun, C. Shao, Y. Chen, H. Hu, R.A. Sheldon, H. Wang, X. Leng, X. Jin, Organometallics 21 (2002) 4350–4355.
[26] N. Sireci, U. Yilmaz, H. Kucukbay, M. Akkurt, Z. Baktir, S. Turktekin, O. Buyukgungor, J. Coord. Chem. 64 (2011) 1894–1902.
[27] H. Lopez-Sandoval, M.E. London-Lemos, R. Garza-Velasco, I. Poblano-Melendez, P. Granada-Macias, I. Gracia-Mora, N. Barba-Behrens, J. Inorg. Biochem. 102 (2008) 1267–1276.
[28] J.R. Ferrer, P.M. Lahti, C. George, P. Oliete, M. Julier, F. Palacio, Chem. Mater. 13 (7) (2001) 2447–2454.
[29] D.H. Brown, R.N. Nuttall, D.W.A. Sharp, J. Inorg. Nucl. Chem. 26 (1964) 1151–1156.
[30] H. Martinez, P. Azavant, M. Loudet, Surf. Sci. 400 (1998) 247–257.
[31] D. Guo, S. Ikeda, K. Saiki, J. Appl. Phys. 99 (2006) 094502.
[32] L.H. Dubois, R.G. Nuzzo, Ann. Rev. Phys. Chem. 43 (1992) 437–463.
[33] J.M. Zadrozny, J. Telser, J.R. Long, Polyhedron 64 (2013) 209–217.
[34] T. Rosu, E. Pahontu, C. Maxim, R. Georgescu, N. Stanica, A. Gulea, Polyhedron 30 (1) (2011) 154–162.
[35] Y.-Q. Hou, D.-M. Zhuang, G. Zhang, M. Zhao, M.-S. Wu, Appl. Surf. Sci. 218 (2003) 98–105.
[36] T. Godin, R. Moncorge, J.-L. Doualan, M. Fromager, K. Ait-Ameur, R.A. Cruz, T. Catunda, J. Opt. Soc. Am. B 29 (5) (2012) 1055–1064.
[37] P. Innocenzi, B. Lebeau, J. Mater. Chem. 15 (2005) 3821–3831.